High order plasmonic Bragg reflection in the metal-insulator-metal waveguide Bragg grating

Junghyun Park, Hwi Kim, and Byoungho Lee*

National Creative Research Center for Active Plasmonics Application Systems
Inter-University Semiconductor Research Center and School of Electrical Engineering
Seoul National University, Gwanak-Gu Sillim-Dong, Seoul, 151-744, Korea
**Corresponding author: byoungho@snu.ac.kr*

http://oeqelab.snu.ac.kr

Abstract: High order plasmonic Bragg reflection in the metal-insulator-metal (MIM) waveguide Bragg grating (WBG) and its applications are proposed and demonstrated numerically. With the effective index method and the standard transfer matrix method, we reveal that there exist high order plasmonic Bragg reflections in MIM WBG and corresponding Bragg wavelengths can be obtained. Contrary to the high order Bragg wavelengths in the case of the conventional dielectric slab waveguide, the results of the MIM WBG exhibit red shifts of tens of nanometers. We also propose a method to design a MIM WBG to have high order plasmonic Bragg reflection at a desired wavelength. The MIM WBG operating in visible spectral regime, which requires quite accurate fabrication process with grating period of 100 to 200 *nm* for the fundamental Bragg reflection, can be implemented by using the higher order plasmonic Bragg reflection with grating period of 400 to 600 *nm* . It is shown that the higher order plasmonic Bragg reflection can be employed to implement a narrow reflection bandwidth as well. We also address the dependence of the filling factor upon the bandgap and discuss the quarter-wave stack condition and the second bandgap closing.

OCIS codes: (240.6680) Surafce plasmons; (230.1480) Bragg reflectors; (230.7390) Waveguides, planar

References and links

1. H. Rather, *Surface Plasmons* (Springer-Verlag, Berlin, 1988).
2. W. L. Barnes, A. Dereux, and T. W. Ebbesen, "Surface plasmon subwavelength optics," Nature **424**, 824-830 (2003).
3. T. Nikolajsen, K. Leosson, and S. I. Bozhevolnyi, "Surface plasmon polariton based modulators and switches operating at telecom wavelengths," Appl. Phys. Lett. **85**, 5833-5835 (2004).
4. A. Boltasseva, T. Nikolajsen, K. Leosson, K. Kjaer, M. S. Larsen, and S. I. Bozhevolnyi, "Integrated optical components utilizing long-range surface plasmon polaritons," J. Lightwave Technol. **23**, 413-422 (2005).
5. S. I. Bozhevolnyi, V. S. Volkov, E. Devaus, and T. W. Ebbesen, "Channel plasmon-polariton guiding by subwavelength metal grooves," Phys. Rev. Lett. **95**, 046802 (2005).
6. P. Berini, "Plasmon-polariton waves guided by thin lossy metal films of finite width: bound modes of symmetric structures," Phys. Rev. B **61**, 10484-10503 (2000).
7. E. N. Economou, "Surface plasmons in thin films," Phys. Rev. **182**, 539-554 (1969).
8. J. J. Burke, G. I. Stegeman, and T. Tamir, "Surface-polariton-like waves guided by thin, lossy metal films," Phys. Rev. B **33**, 5186-5201 (1986).
9. R. Zia, M. D. Selker, P. B. Catrysse, and M. Brongersma, "Geometries and materials for subwavelength surface plasmon modes," J. Opt. Soc. Am. A **21**, 2442-2446 (2004).
10. J. A. Dionne, L. A. Sweatlock, and H. A. Atwater, "Planar metal plasmon waveguides: Frequency-dependent dispersion, propagation, localization, and loss beyond the free electron model," Phys. Rev. B **72**, 075405 (2005).

#89396 - $15.00 USD Received 5 Nov 2007; revised 28 Dec 2007; accepted 28 Dec 2007; published 4 Jan 2008

11. J. A. Dionne, L. A. Sweatlock, and H. A. Atwater, "Plasmon slot waveguides: Towards chip-scale propagation with subwavelength-scale localization," Phys. Rev. B **73**, 035407 (2006).
12. I.-M. Lee, J. Jung, J. Park, H. Kim, and B. Lee, "Dispersion characteristics of channel plasmon polariton waveguides with step-trench-type grooves," Opt. Express **15**, 16596-16603 (2007).
13. A. Boltasseva, S. I. Bozhevolnyi, T. Nikolajsen, and K. Leosson, "Compact Bragg gratings for long-range surface plasmon polaritons," J. Lightwave Technol. **24**, 912-918 (2006).
14. B. Wang and G. P. Wang, "Plasmon Bragg reflectors and nanocavities on flat metallic surfaces," Appl. Phys. Lett. **87**, 013107 (2005).
15. A. Hosseini and Y. Massoud, "A low-loss metal-insulator-metal plasmonic Bragg reflector," Opt. Express **14**, 11318-11323 (2006).
16. Z. Han, E. Forsberg, and S. He, "Surface plasmon Bragg gratings formed in metal-insulator-metal waveguides," IEEE Photon. Technol. Lett. **19**, 91-93 (2007).
17. A. Hosseini and Y. Massoud, "Subwavelength plasmonic Bragg reflector structures for on-chip optoelectronic applications," International Symposium on Circuits and Systems, New Orleans, LA, 2283-2286 (2007).
18. J. A. Dionne, H. J. Lezec, and H. A. Atwater, "Highly confined photon transport in subwavelength metallic slot waveguides," Nano Letters **6**, 1928-1932 (2006).
19. D. Z. Lin, C. K. Chang, Y. C. Chen, D. L. Yang, M. W. Lin, J. T. Yeh, J. M. Liu, C. H. Kuan, C. S. Yeh, and C. K. D. Lee, "Beaming light from a subwavelength metal slit surrounded by dielectric surface gratings," Opt. Express **14**, 3503-3511 (2006).
20. M. G. Moharam and T. K. Gaylord, "Rigorous coupled-wave analysis of planar-grating diffraction," J. Opt. Soc. Am. A **71**, 811-818 (1981).
21. M. G. Moharam, E. B. Grann, and D. A. Pommet, "Formulation for stable and efficient implementation of the rigorous coupled-wave analysis of binary gratings," J. Opt. Soc. Am. A **12**, 1067-1076 (1995).
22. P. Lalanne, "Improved formulation of the coupled-wave method for two-dimensional gratings," J. Opt. Soc. Am. A **14**, 1592-1598 (1997).
23. H. Kim, I.-M. Lee, and B. Lee, "Extended scattering-matrix method for efficient full parallel implementation of rigorous coupled-wave analysis," J. Opt. Soc. Am. A **24**, 2313-2327 (2007).
24. B. E. A. Saleh and M. C. Teich, *Fundamentals of Photonics*, 2nd ed. (Wiley Intersceince, Hoboken, NJ, 2007).

1. Introduction

Surface plasmon polaritons (SPPs) are quasi-particles resulting from coupling of electromagnetic waves with oscillations of conduction electrons in a metal and propagate along the interface between a dielectric and a metal. The SPP-based photonic devices have been attracting lots of attention of researchers due to their ability of confining the light in subwavelength scale [1, 2]. Various kinds of reports have been published for the basic waveguide utilizing SPPs, directional couplers and splitters, and even modulators utilizing electro/thermo effect [3, 4].

As the most fundamental and basic photonic devices, the SPP waveguide structures such as the insulator-metal-insulator (IMI) waveguides and the metal-insulator-metal (MIM) waveguides have been examined theoretically and experimentally [5-12]. It is well known that the IMI waveguide exhibits less propagation loss, giving rise to longer propagation length than the MIM waveguide [6]. On the other hand, from a view point of confining light wave, the MIM waveguide is better than the IMI waveguide [9]. Meanwhile, as the wavelength-dependent photonic device, there have been lots of researches on Bragg gratings on the IMI waveguide. Boltasseva *et al*. proposed compact and efficient Bragg gratings for long-range SPP operating around $1550\,nm$ by introducing periodic thickness modulation of thin metal stripes embedded in a dielectric [13]. There also have been many efforts in examining Bragg gratings on the MIM waveguides [14-17]. Wang and Wang proposed metal heterostructure SPP Bragg reflectors and nano cavities on flat metallic surfaces [14]. Hosseini and Massoud suggested a low-loss plasmonic Bragg reflector consisting of alternatively stacked MIM waveguides with different dielectric materials [15]. Han *et al.* devised surface plasmon Bragg gratings formed by a periodic variation of the width of the insulator in MIM waveguide [16]. Hosseini and Massoud also discussed differences between the MIM waveguide Bragg gratings

#89396 - $15.00 USD Received 5 Nov 2007; revised 28 Dec 2007; accepted 28 Dec 2007; published 4 Jan 2008

(WBGs) of the index modulation and that of the thickness modulation [17]. Those structures have grating periods of about 400 to 600 nm.

While the structures of aforementioned papers are designed to operate on the range of telecommunications, understanding the behavior of MIM waveguide in the visible spectral regime is regarded as of great importance as well. To accomplish the fundamental Bragg reflection in visible range, the period of unit cell needs to be reduced to a range of 100~200 nm. Furthermore, since the effective refractive index increases with decrease of the operating wavelength, it is required to fabricate a periodic structure with much shorter period, such as below 100 nm. The dielectric grating on the metal substrate can be patterned via the electron beam lithography method or the focused ion beam method, which bring about inevitable roundish edge effect [18, 19]. In analogy to the higher order Bragg reflection in the fiber Bragg grating, the higher order plasmonic Bragg reflection can be utilized to implement the MIM WBG operating in visible spectral regime. However, due to the dispersive property of metal used in plasmonic structure and the high confinement of the electromagnetic field, it is expected that the high order plasmonic Bragg reflection has unique property compared to the high order photonic Bragg reflection in the dielectric material. Therefore, making use of high order plasmonic Bragg reflection in MIM WBG seems to be a worthwhile subject. In addition, one may be inclined to build the MIM WBG with narrow reflection bandwidth for filtering applications. It is well known that a periodic structure with small index contrast exhibits narrow bandgap. It would be of interest to compare the behavior of the MIM WBG with small index contrast and the higher order plasmonic Bragg reflection.

In this paper, we investigate the high order plasmonic Bragg reflection in the MIM WBG. First we review briefly the fundamental properties of the MIM waveguide and its dependency upon various geometrical and material parameters. Then, considering the material and waveguide dispersion, we suggest a method to find out the high order plasmonic Bragg wavelength using a graphical method. With the effective index method (EIM) and the rigorous coupled-wave analysis (RCWA) [20-23], we examine the reflection from and the transmission through the MIM WBG. Next, we propose a method for designing a MIM WBG with the high order plasmonic Bragg reflection at a required wavelength. As applications, we suggest a MIM WBG operating in visible or telecommunication spectral regime with a narrow reflection bandwidth. Finally, we study the property of the bandgap in the MIM WBG as a function of the filling factor. It can be shown that, when the ratio between the lengths of two different MIM waveguides is inversely proportional to that of the effective refractive index, the second bandgap is closed.

2. Fundamental properties of the MIM waveguide

Figure 1 illustrates a schematic diagram of a MIM waveguide, which consists of a dielectric core with thickness t surrounded by two half-infinite metal claddings. Since we are interested in behavior of the plasmonic wave, it is assumed that the electromagnetic (EM) field is of p-polarization so that E_x, H_y and E_z have non-zero values whereas H_x, E_y and H_z are all zero.

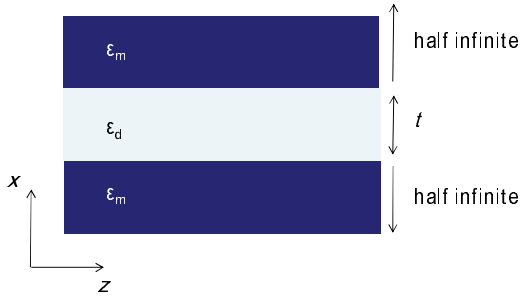

Fig. 1. Schematic diagram of a metal-insulator-metal waveguide

#89396 - $15.00 USD Received 5 Nov 2007; revised 28 Dec 2007; accepted 28 Dec 2007; published 4 Jan 2008

From continuity of transverse electric field E_z and H_y along the interface between two different media, we obtain the dispersion relation as follows [11] :

$$\frac{\kappa_m}{\varepsilon_m} = -\frac{\kappa_d}{\varepsilon_d} \tanh\left(\frac{t}{2}\kappa_d\right), \tag{1}$$

where ε_d is the dielectric constant of the dielectric core, ε_m the dielectric function of metal cladding, and κ_d and κ_m are the transverse (*x*-direction) wave number in the core and the cladding, respectively. To describe the dielectric function for silver, we employ the free electron model which can be expressed as follows:

$$\varepsilon_{silver}(\omega) = \varepsilon_\infty - \frac{\omega_p^2}{\omega(\omega + i\gamma)}, \tag{2}$$

where ε_∞ represents the dielectric constant at infinite angular frequency and is chosen to have 3.70. ω_p stands for the bulk plasma frequency with the value of 9eV. γ means the oscillation damping of electrons and the value is 0.018eV. These parameters are chosen so that they describe the angular frequency dependency of silver with best fit for the free-space wavelength from 400 to 2000 nm. Note that we express the angular frequency in a form of photon energy by multiplying the Plank's constant $\hbar$ [14, 16].

Due to symmetry in the given structure, there can be two possible plasmonic modes in the MIM waveguide - one is the anti-symmetric mode and the other one is the symmetric mode. The terminology we use here is based on the charge distribution or the longitudinal electric field (E_z). Hence both the transverse electric field (E_x) and the transverse magnetic field (H_y) exhibit the symmetric distribution at the anti-symmetric mode and the anti-symmetric distribution at the symmetric mode. The symmetric mode in MIM waveguide exhibits cut-off when its thickness goes below a cut-off thickness, which is typically shown to be hundreds of nanometers [11]. Since our configuration deals with the MIM waveguide with the thickness below cut-off thickness of the symmetric mode, we only take the anti-symmetric mode into account. From the momentum conservation condition in each medium, we can induce relations between the transverse wave numbers κ_d, κ_m and the longitudinal (*z*-direction) wave number β [1]:

$$-\kappa_d^2 + \beta^2 = \varepsilon_d k_0^2 = \varepsilon_d \left(\frac{\omega}{c_0}\right)^2, \tag{3.a}$$

$$-\kappa_m^2 + \beta^2 = \varepsilon_m k_0^2 = \varepsilon_m \left(\frac{\omega}{c_0}\right)^2, \tag{3.b}$$

where c_0 is the speed of light in the free space. ω is the angular frequency of the photon at the free space wavelength λ_0 and its wave number is denoted by k_0. Combining Eqs. (1) and (3) determines β, κ_d and κ_m. The real part of β normalized with k_0 is called the effective refractive index n_{eff} and plays an important role in designing the MIM WBG. The inverse of the imaginary part of β multiplied by one half is referred to as the propagation length, at which the propagating field intensity (or, square of field) decays by e^{-1} (0.37). The skin depth through the cladding is defined as the inverse of the real part of κ_m, which is related to the modal size.

#89396 - $15.00 USD Received 5 Nov 2007; revised 28 Dec 2007; accepted 28 Dec 2007; published 4 Jan 2008

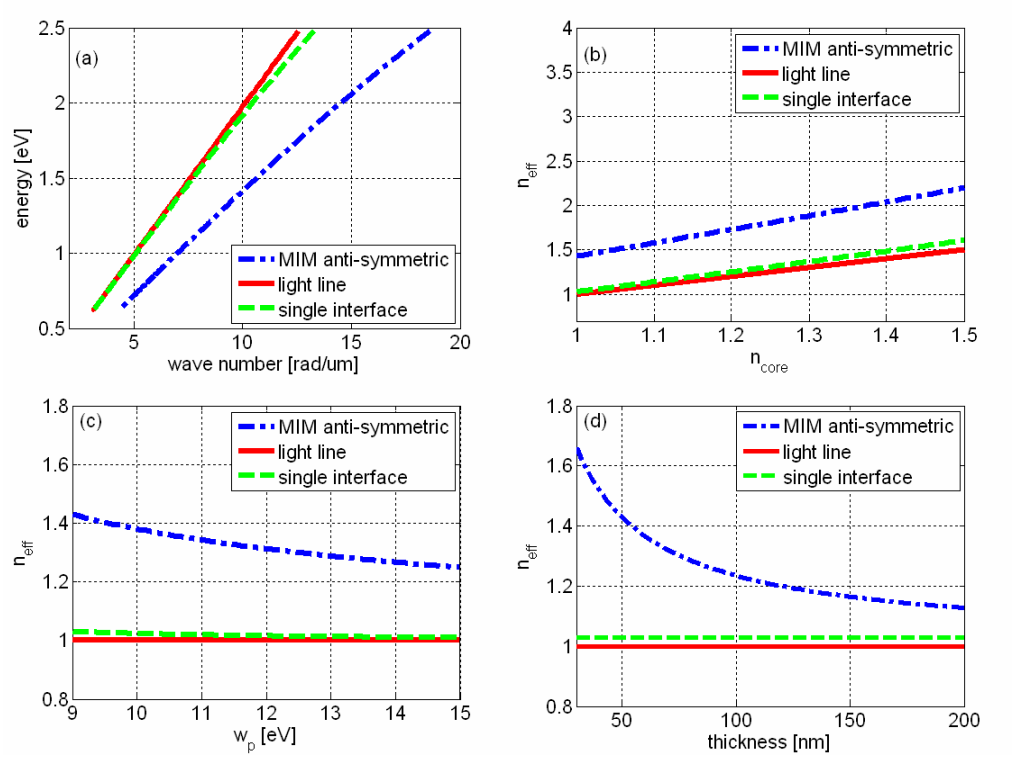

Fig. 2. Basic properties of the anti-symmetric mode in the MIM waveguide. (a) Dispersion relation (t =50 nm , ε_d =1, and ω_p = 9eV). Dependence of the effective refractive index at λ =633 nm upon (b) the refractive index of the dielectric core (t =50 nm , ω_p = 9eV), (c) the bulk plasma frequency of the metal cladding (t =50 nm , ε_d =1), and (d) the thickness of the dielectric core (ε_d =1, ω_p = 9eV)

Before discussion on the high order plasmonic Bragg reflection at given structure, it would be of importance to review briefly the dependence of n_{eff} of the anti-symmetric mode in the MIM waveguide upon various geometrical parameters such as the operating wavelength, the type of the metal cladding, the thickness and the dielectric constant of the dielectric core. Figure 2(a) shows the dispersion relation of the anti-symmetric mode in the MIM waveguide. The dispersion relation curve of the anti-symmetric mode lies to right side of the dispersion curve of the single interface. It is known that as the thickness of the dielectric core changes from infinity to tens of nanometers, the dispersion moves from the single interface line to right side of it. Figures 2(b)-(d) illustrate n_{eff} as a function of the geometrical parameters. n_{eff} of the anti-symmetric mode for each case is always higher than that of the single interface. By alternatively stacking MIM waveguides with different geometrical parameters, we can build up the MIM WBG. Merits and demerits of each type – the dielectric core index modulation, the metal cladding modulation and the thickness of the dielectric core modulation – have been discussed widely in some papers [14-17]. The MIM WBG using the modulation of the dielectric core has strength of low loss with high light confinement even though the fabrication of it would be more difficult than other types of MIM WBG. Hence we are going to discuss the high plasmonic Bragg reflection for the MIM WBG using the modulation of the dielectric core. The research about the high order plasmonic Bragg reflection for other types of the MIM WBG is in the process and the results will be reported in a next paper.

#89396 - $15.00 USD Received 5 Nov 2007; revised 28 Dec 2007; accepted 28 Dec 2007; published 4 Jan 2008

3. High order plasmonic Bragg reflection in the MIM WBG

The schematic diagram of a MIM WBG with periodic modulation of the core index is illustrated in Fig. 3. d_1 and d_2 stand for the lengths of the MIM waveguides with the core indices of ε_{d1} and ε_{d2}, respectively. Λ is the period of the gratings in the waveguide.

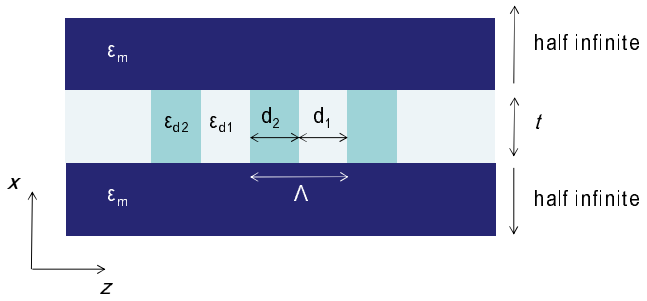

Fig. 3. Schematic diagram of a metal-insulator-metal waveguide Bragg grating with periodic modulation of the core index

The conventional condition for Bragg reflection is governed by

$$q\lambda_{B,q} = 2\Lambda\, \tilde{n}_{eff}\Big|_{\lambda_{B,1}}, \tag{4}$$

where q is an integer which represents the order of the Bragg reflection and $\lambda_{B,q}$ is the q-th order Bragg wavelength at which reflectance from and transmittance through the waveguide gets almost unity and zero, respectively. $\tilde{n}_{eff}$ is the averaged effective refractive index at the fundamental Bragg wavelength, which is defined as

$$\tilde{n}_{eff}\Big|_{\lambda_{B,1}} = \frac{d_1\, n_{eff,1}\Big|_{\lambda_{B,1}} + d_2\, n_{eff,2}\Big|_{\lambda_{B,1}}}{d_1 + d_2}. \tag{5}$$

In the conventional waveguides, we can obtain high order plasmonic Bragg wavelengths by simply dividing the fundamental Bragg wavelength in Eq. (4) with multiple integers. However, this is valid only when the averaged effective refractive index remains almost constant with the value at fundamental Bragg wavelength meaning next to zero dispersion in the waveguide.

When considering the highly dispersive property of MIM waveguide, however, we need to invoke a graphical method to anticipate the location of high order plasmonic Bragg wavelengths. Instead of Eq. (4) we adopt an alternative equation as follows:

$$n_{eff}(\lambda) = \frac{q\lambda}{2\Lambda} \tag{6}$$

Note that in Eq. (6), the averaged effective refractive index is not a constant but a function of the operating wavelength λ. A point of intersection between the left-hand side of Eq. (6) and the right-hand side of Eq. (6) represents that the high order plasmonic Bragg reflection condition is satisfied, so that at the wavelength of horizontal axis value of the graph of the intersection the high order plasmonic Bragg reflection occurs.

Figure 4(a) shows the numerical results. The MIM WBG consists of two different MIM waveguides with the core indices of 1.00 and 1.20, respectively. The thickness is $50\,nm$ and the dielectric function of the metal cladding is from Eq. (2). For each MIM waveguide, n_{eff} at the operating wavelength of $1550\,nm$ is read as 1.378 and 1.656, respectively. The filling factor, or duty ratio is defined as $f = d_1/(d_1 + d_2) = d_1/\Lambda$ and its contribution to the behavior

#89396 - $15.00 USD Received 5 Nov 2007; revised 28 Dec 2007; accepted 28 Dec 2007; published 4 Jan 2008

of the MIM WBG will be discussed later. For now we assume that the filling factor is 0.5, namely the ratio between the lengths of two MIM waveguides is 1:1. With the averaged effective refractive index of 1.517 at the operating wavelength of 1550 *nm*, the period of the gratings for the fundamental Bragg wavelength of 1550 *nm* is obtained as 510 *nm*. It is observed in a cyan-colored line in Fig. 4(a) that in the case of the conventional dielectric slab waveguide (DSW), the dispersion is negligible so that the high order Bragg wavelengths are obtained as about 775 *nm* and 517 *nm*, which are in good agreement with the result of Eq. (4).

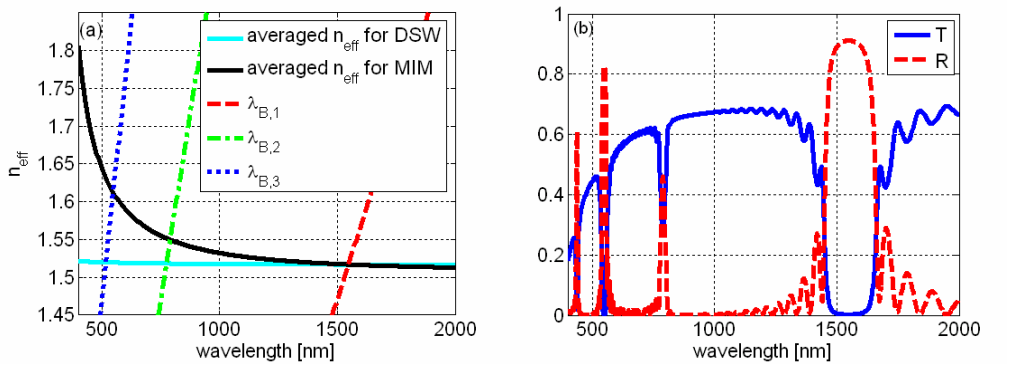

Fig. 4. (a) Graphical method to find the high order plasmonic Bragg wavelengths. (b) Transmission spectrum (solid line) and reflection spectrum (dashed line). $t = 50nm$, $\varepsilon_{d1} = 1.00$, $\varepsilon_{d2} = 1.44$, $\Lambda = 510nm$, and $f = 0.5$.

As a matter of fact, however, the second and third order plasmonic Bragg wavelengths exhibit red shift in the case of the MIM WBG. From Fig. 4(a), it is seen that the second and third order plasmonic Bragg reflections occur at the operating wavelength of 789 *nm* and 548 *nm*, which are shifted about 14 *nm* and 31 *nm* from the result of non-dispersive assumption. This is due to the increase of the averaged effective refractive index with decrease of the operating wavelength. To check out the high order plasmonic Bragg reflection, we calculated the reflectance and transmittance spectra using the RCWA [20-23], and the result is plotted in Fig. 4(b). We used 201 plane waves and the computation cell with size of 500 *nm*. It should be pointed that we have checked agreement between property of the eigenmode obtained from the RCWA and that from the analytical solution in Eq. (1). The number of cells is 20. The effect of the number of cells upon reflection and transmission spectra has been reported [17]. From Fig. 4(b), it is observed that the second and third order Bragg reflections take place at the wavelengths of 789 *nm* and 548 *nm* with reflectivity of 48.8% and 83.5%, respectively. And their bandwidths defined by the full width at half-maximum (FWHM) are obtained as 22 *nm* and 20 *nm*. It is also noteworthy that the bandwidth is narrow at the high order plasmonic Bragg reflection, which suggests an application for the design of narrow stop bandgap device. This will be discussed in the following section in this paper. Figures 5(a)-(c) illustrate the field distribution in the MIM WBG at the fundamental Bragg wavelength, the second order Bragg wavelength, and the third order Bragg wavelength, respectively. It becomes evident that the higher order plasmonic reflections occur at the higher order Bragg wavelengths of 789 *nm* and 548 *nm*. It is also observed that at the second order Bragg wavelength the reflection is quite weak and the transmission is not negligible. Thus the second order Bragg reflection does not seem to be appropriate for practical applications. Through this paper, therefore, applications utilizing the higher order plasmonic Bragg reflection mainly deal with the third order Bragg reflection.

#89396 - $15.00 USD Received 5 Nov 2007; revised 28 Dec 2007; accepted 28 Dec 2007; published 4 Jan 2008

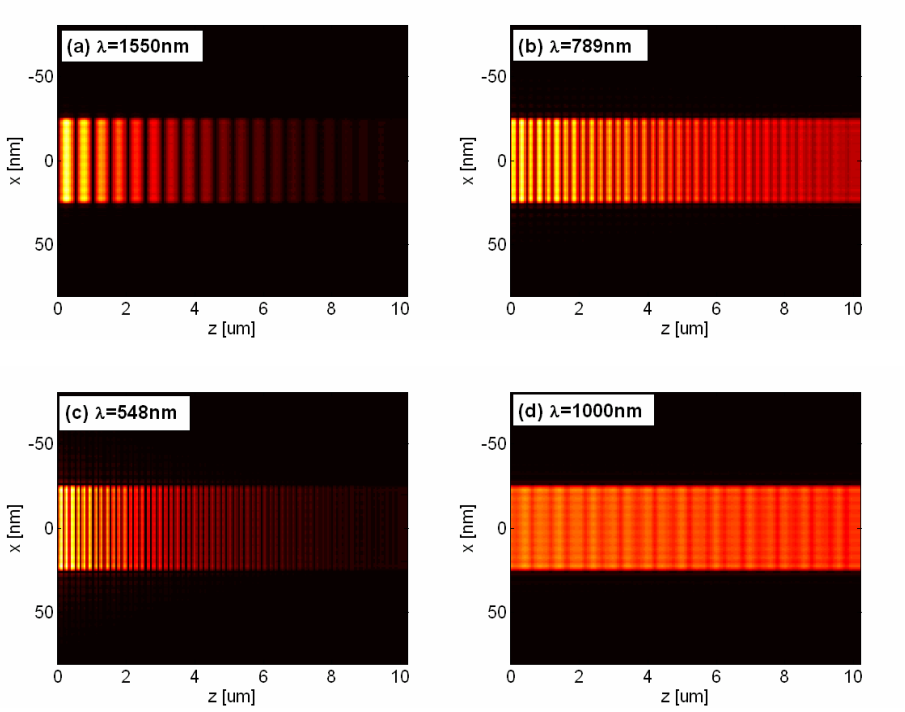

Fig. 5. Intensity of the tangential component of the electric field ($|E_x|^2$) of the MIM WBG with (a) the fundamental Bragg wavelength, (b) the second order Bragg wavelength, (c) the third order Bragg wavelength, and (d) wavelength of 1000 *nm* in the passband. The geometrical parameters are the same as those in the Fig. 4.

So far we discussed the alternatively stacked heterostructure of two different MIM waveguides with finite number of cell. It would be of great interest to investigate the Bloch mode that can exist in the infinitely stacked heterostructure. The dispersion relation is given by

$$\cos(K\Lambda) = \mathrm{Re}\left\{\frac{1}{t(\omega)}\right\} = \frac{\left(n_{eff,1}+n_{eff,2}\right)^2}{4n_{eff,1}n_{eff,2}}\cos(\varphi_1+\varphi_2) - \frac{\left(n_{eff,1}-n_{eff,2}\right)^2}{4n_{eff,1}n_{eff,2}}\cos(\varphi_1-\varphi_2), \quad (7)$$

where ω is the angular frequency and K is the Bloch wave number [24]. $t(\omega)$ is the transmittance from unit cell. φ_1 and φ_2 are the phases introduced by two layers of a unit cell and defined as $\varphi_i = k_0 n_{eff,i} d_i$ ($i = 1, 2$). Figure 6 illustrates the Bloch wave number as a function of the angular frequency. Note that abscissa is normalized with π/Λ and ordinate is scaled with the Bragg frequency $\omega_B = \pi c_0 / \tilde{n}_{eff}\Lambda$, where $\tilde{n}_{eff}$ is the averaged effective refractive index at the wavelength of 1550 *nm* . As predicted, the fundamental plasmonic bandgap takes place at the Bragg angular frequency. If there were no dispersion in this structure, the high order plasmonic bandgap would occur at the integer multiple of the Bragg angular frequency. As can be seen in Fig. 6, however, it is observed that the high order plasmonic bandgap happens at the smaller angular frequency than integer multiple. The result supports that there is red shift not only in finite Bragg grating but also in infinite bandgap structure.

#89396 - $15.00 USD Received 5 Nov 2007; revised 28 Dec 2007; accepted 28 Dec 2007; published 4 Jan 2008

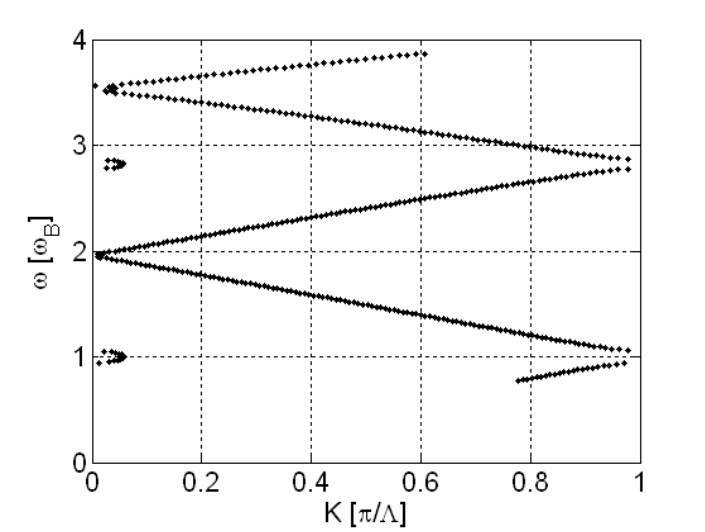

Fig. 6. Dispersion diagram of the alternatively stacked MIM waveguide structure

4. Application of the higher order plasmonic Bragg reflection – MIM WBG at the visible spectral regime and MIM WBG with narrow reflection band

Let us now consider an application of high order plasmonic Bragg reflection in MIM waveguide. We can benefit in mainly two ways from the high order plasmonic Bragg reflection: one is easiness in fabrication, and the other one is designing devices with narrow reflection spectra. The grating period for high order plasmonic Bragg reflection at a desired wavelength can be easily obtained from Eq. (4). Note that we can obtain high order plasmonic Bragg reflection in the MIM waveguide by just multiplying the period of cell by integer. For example, a Bragg grating is designed for third order Bragg reflection at the wavelength of $532\,nm$ and the reflection and the transmission spectra (solid blue line) are depicted in Figs. 7(a) and (b), respectively. Since the averaged effective refractive index at the wavelength of $532\,nm$ is obtained as 1.623, the period of the grating is designed to be $492\,nm$ for the third order Bragg reflection.

On the other hand, the Bragg reflection at the wavelength of $532\,nm$ can be implemented by using the fundamental Bragg reflection with the grating period of $164\,nm$. The reflection and the transmission spectra (dashed red line) of the fundamental Bragg reflection are also illustrated in Figs. 7(a) and (b), respectively. It should be mentioned that the number of periodic cell (#) is chosen in such a way that two MIM WBGs have the same total grating length ($9.84\,\mu m$). In Table 1, we summarize the characteristics of two MIM WBGs such as the center wavelength of Bragg reflection (λ_c), the bandwidth ($\Delta\lambda$), the grating strength ($\Delta\lambda/\lambda_c$), the reflection at λ_c (R), the transmission at λ_c (T), and the propagation loss at λ_c (L). It is observed that the grating strength of the third order Bragg reflection is weaker about threefold than that of the fundamental Bragg reflection. The third order Bragg reflection also exhibits less reflection and more propagation loss than those of the fundamental Bragg reflection. However we give attention to the fact that in the case of using the third order Bragg reflection, the reflection is more than 80% and the transmission exhibits less than 1%, which still suggests the adequate bandgap property. Considering the easiness of fabrication process, therefore, we can benefit from using the third order Bragg reflection to implement the MIM WBG having bandgap at visible spectral regime.

As another application of the high order plasmonic Bragg reflection, we propose a method to implement a Bragg grating with a narrow reflection band. Various methods to implement a Bragg grating with a narrow transmission band have already been reported [14-

#89396 - $15.00 USD Received 5 Nov 2007; revised 28 Dec 2007; accepted 28 Dec 2007; published 4 Jan 2008

16]. They used an intentionally adopted defect mode in periodic gratings, so that the device exhibits both a broad reflection band and a sharp transmission window inside the band. Meanwhile, from the reflection and the transmission spectrum in Fig. 4(b), it is seen that high order plasmonic Bragg reflection exhibits much narrow reflection bandwidth than that of fundamental Bragg reflection. This is due to the second term in Eq. (7), which acts as a perturbation of Bragg reflection band. Taking this property into account, we build the high order plasmonic Bragg grating with narrow reflection band by simply multiplying the period of the unit cell with integer. Figures 8(a) and (b) illustrate the reflection from and the transmission through the MIM WBGs designed for a center frequency of 1550 *nm* using different types of gratings. The dashed red lines in Fig. 8 correspond to results of the third order Bragg reflection. It is seen that unlike the fundamental Bragg reflection at 1550 *nm* shown in Fig. 4(b), the third order Bragg reflection exhibits the quite narrow bandwidth. Other properties are summarized in Table 2.

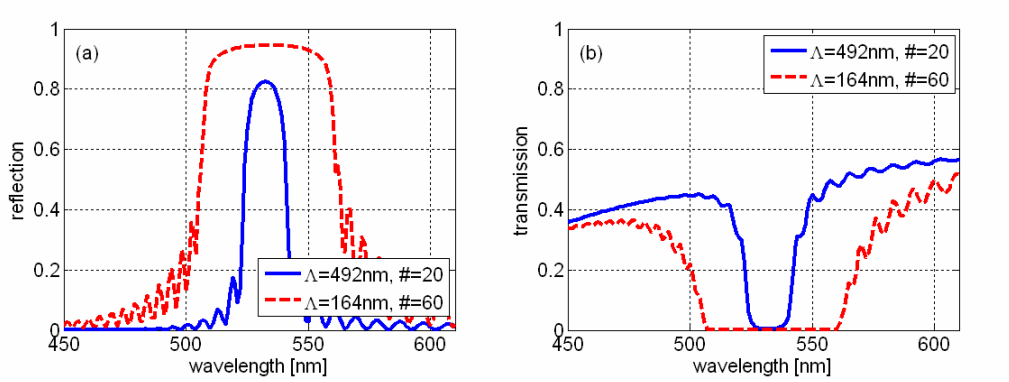

Fig. 7. (a) Reflection and (b) transmission spectra of the MIM WBG with the fundamental Bragg reflection (dashed red line) and the third order Bragg reflection (solid blue line)

Table 1. Bandgap properties of the MIM WBG having bandgap at 532 *nm*

	$\Lambda\,(nm)$	#	$\lambda_c\,(nm)$	$\Delta\lambda\,(nm)$	$\Delta\lambda/\lambda_c$	R	T	L
1st order	164	60	532	57.5	0.1081	0.9449	0.0000	0.0551
3rd order	492	20	532	17.7	0.0333	0.8243	0.0038	0.1719

It is well known that the less index contrast the MIM WBG gets, the narrower the bandwidth becomes [15]. In order to compare two methods to make a narrow reflection band, we also investigate the reflection spectrum for the MIM WBG with low index contrast. The MIM waveguides with the core indices of 1.07 and 1.13 have the effective refractive indices of 1.475 and 1.558 at the wavelength of 1550 *nm*, respectively. The grating period of 511 *nm* is chosen so that the fundamental Bragg reflection takes place at the wavelength of 1550 *nm*. The bandwidth is related to the normalized index contrast [15].

$$\Delta n_{norm} = \left| \frac{n_{eff,2} - n_{eff,1}}{n_{eff,2} + n_{eff,1}} \right| \tag{8}$$

The normalized index contrast is obtained as 0.0274 for the MIM WBG with the core indices of 1.07 and 1.13. For the MIM waveguide with the core index of 1.00 and 1.20, the normalized index contrast is 0.0915. To balance the grating strength, we set the total grating length to be near the same for the fundamental Bragg reflection with the low index contrast,

#89396 - $15.00 USD Received 5 Nov 2007; revised 28 Dec 2007; accepted 28 Dec 2007; published 4 Jan 2008

and for the third order Bragg reflection with the high index contrast. In the former case the number of the gratings with period of 511 *nm* is 60, resulting in the total grating length of 30.660 μm . In the latter case, the grating period with 1530 *nm* (510 multiplied by 3) is stacked 20 times, giving rise to the total grating length of 30.600 μm . The solid blue lines in Fig. 8 correspond to the low index contrast. It is seen that the reflection bandwidths for the fundamental Bragg reflection with low index contrast and the third order Bragg reflection with high index contrast are obtained as 60nm and 61nm, respectively. And other properties such as reflection, transmission, and propagation loss are quite similar. It is noteworthy that the fundamental Bragg reflection with reduced cell number does not exhibit comparable narrow bandwidth. As evident from Fig. 8, the third order Bragg reflection with the high index contrast can be used to develop a narrow reflection band with similar performance for the fundamental Bragg reflection with the low index contrast. Although there is trade-off of easiness in fabrication for gratings with the long period and the high contrast against gratings with the short period and the low contrast, one thing to be emphasized is that the higher order plasmonic Bragg reflection gives us flexibility in design scheme.

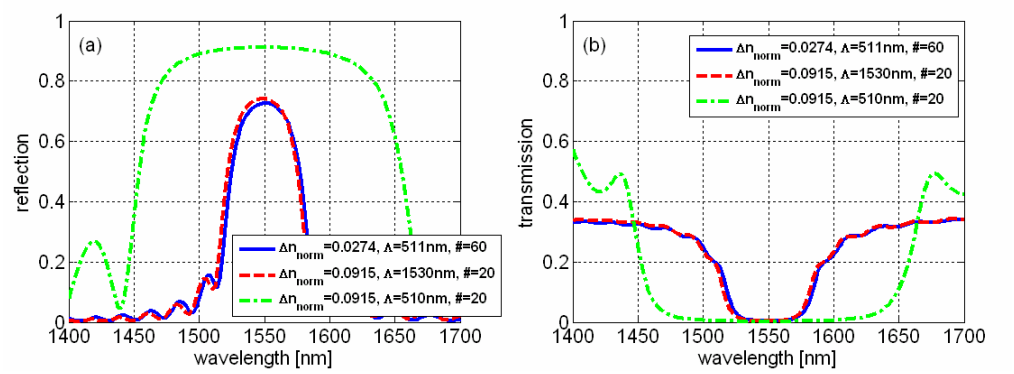

Fig. 8. (a) Reflection and (b) transmission spectra of the MIM WBG with the low index contrast fundamental Bragg reflection (solid blue line), the high index contrast third order Bragg reflection (dashed red line), and the high index contrast fundamental Bragg reflection with reduced cell number (dash-dotted green line)

Table 2. Bandgap properties of the MIM WBG having bandgap at 1550 *nm*

	$\Lambda\,(nm)$	#	$\lambda_c\,(nm)$	$\Delta\lambda\,(nm)$	$\Delta\lambda/\lambda_c$	R	T	L
Low index contrast	511	60	1550	60	0.0387	0.7268	0.0039	0.2693
3rd order Bragg reflection	1530	20	1550	61	0.0394	0.7414	0.0036	0.2550
Reduced cell period	510	20	1550	203	0.1310	0.9114	0.0026	0.0860

5. Second bandgap closing and the filling factor

So far, the filling factor has been chosen to be 0.5. In this section, we'd like to discuss the dependence of the behavior of the high order plasmonic Bragg reflection on the filling factor in detail. Figure 9(a) illustrates the bandgap calculated by the Bloch theorem as a function of the filling factor. As in Fig. 6, the ordinate is normalized with the Bragg angular frequency at

#89396 - $15.00 USD Received 5 Nov 2007; revised 28 Dec 2007; accepted 28 Dec 2007; published 4 Jan 2008

the wavelength of 1550 nm. Recall that the we have assumed $n_{eff,1}$ is lower than $n_{eff,2}$. Since the period of the unit cell is fixed, the averaged effective refractive index decreases with increase of the filling factor, resulting in increase of the position of the bandgap in the frequency domain. This is shown in Fig. 9(a). It is also observed that at the filling factor around 0.55, the second order bandgap disappears. This is referred to as the second bandgap closing. To understand this phenomenon and get a physical insight, we investigate the ratio of the effective refractive index as a function of wavelength. The result is depicted in Fig. 9(b).

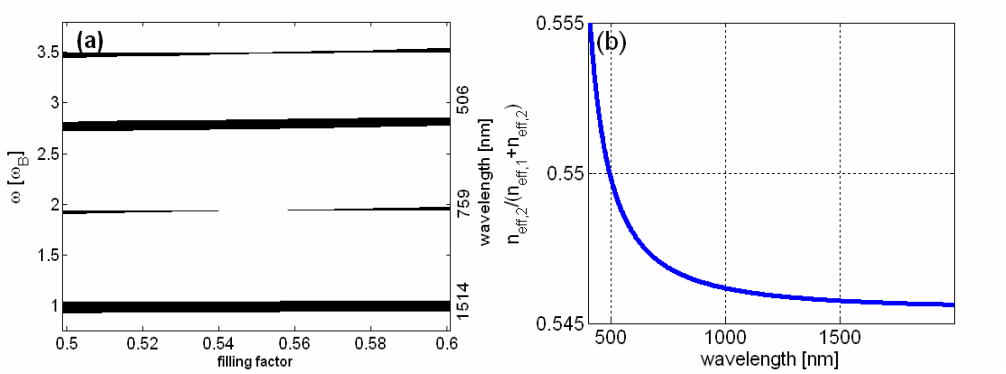

Fig. 9. (a) Bandgap diagram of the infinite periodic structure as a function of filling factor. (b) Ratio between $n_{eff,1}$ and $n_{eff,2}$ as a function of the operating wavelength

Considering that the second order Bragg reflection happens at around wavelength of 789 nm, we obtain the ratio of effective refractive index as 0.548, which lies inside the second bandgap closing region in Fig. 9(a). With simple calculation it can be shown that the filling factor of 0.548 means that the ratio between d_1 and d_2 is inversely proportional to the ratio of the effective refractive index at the wavelength of the second order Bragg reflection. This relation can be expressed as $d_1 : d_2 = n_{eff,2} : n_{eff,1}$, which can be regarded as condition for the quarter-wave stack. It is well known that even bandgap closing takes places at a conventional periodic structure of the quarter-wave stack. This is due to the fact that the wave reflected by the first half layer of a unit cell experiences the phase shift of 3π, so that it interferes destructively with the wave reflected by the total unit cell and prevents the Bragg reflection. The result shown in Fig. 9(a) suggests that a plasmonic periodic structure of the quarter-wave stack also suppresses the second order Bragg reflection.

To verify the second order bandgap closing at the filling factor of 0.548, we investigate the reflection and transmission spectra. Figure 10(a) illustrates the reflection and transmission spectra for the MIM WBG with the filling factor of 0.548. It is observed that the second order Bragg reflection disappears, which agrees well with the aforementioned discussion. We also survey the Bloch wave number and bandgap and show the result in Fig. 10(b). Note that the ordinate is normalized with the Bragg angular frequency for the effective refractive index at the wavelength of 1550 nm. It can be seen that the curves for Bloch wave near the second order bandgap adjoin to each other, giving rise to closing of the second bandgap. Based on the results above, we reason that when the ratio of the length for each region is inversely proportional to the effective refractive index at the specific high order Bragg wavelength, the gratings perform as a quarter-wave stack, leading to a second order bandgap closing. This property can be used to design a grating structure without the second order Bragg reflection.

#89396 - $15.00 USD Received 5 Nov 2007; revised 28 Dec 2007; accepted 28 Dec 2007; published 4 Jan 2008

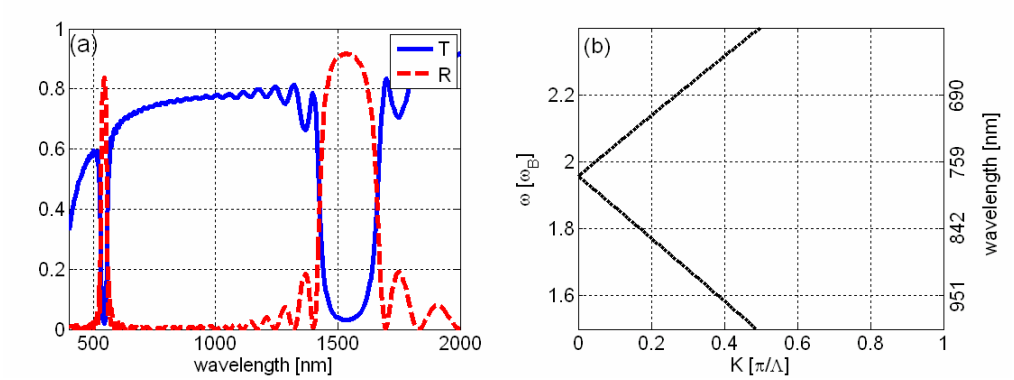

Fig. 10. (a) Reflection (R) and transmission (T) spectra and (b) Bloch diagram for the MIM WBG with the filling factor of 0.548

6. Conclusion

In this paper, we revealed that the high order plasmonic Bragg reflection takes places in the MIM WBG and presented a method to find the high order plasmonic Bragg wavelength based on the graphical method. Unlike the high order Bragg wavelengths in the case of the conventional DSW, they exhibited red shifts of 14 *nm* and 31 *nm* from the result of non-dispersive assumption for the second and the third order plasmonic Bragg wavelengths, respectively. This was also verified with the reflection and the transmission spectra from the RCWA and the Bloch diagram from the Bloch wave analysis. As applications using the high order plasmonic Bragg reflection, we suggested the MIM WBG at the visible spectral regime without gratings of not too short period, which had the third order stop band at the wavelength of 532 *nm* with the grating period of 492*nm* . We also proposed the MIM WBG with a narrow reflection band at the telecommunication wavelength (1550 *nm*) with the bandwidth of 61 *nm* , which was comparable with the MIM WBG with the low index contrast and the short period (60 *nm*). Finally the dependence of the filling factor upon the bandgap was addressed and the quarter-wave stack condition and the second bandgap closing were discussed.

Acknowledgment

The authors acknowledge the support by the Ministry of Science and Technology of Korea and Korea Science and Engineering Foundation through the Creative Research Initiative Program (Active Plasmonics Application Systems).

#89396 - $15.00 USD Received 5 Nov 2007; revised 28 Dec 2007; accepted 28 Dec 2007; published 4 Jan 2008